

## The reconstruction of NEON

---

**Chengyu Shao,<sup>a,\*</sup> Yudong Cui,<sup>a</sup> Pingzheng Dong,<sup>a</sup> Yunlei Huang,<sup>a</sup> Sujie Lin,<sup>a</sup> Yihan Liu,<sup>a</sup> Zijian Qiu,<sup>a</sup> Yihan Shi,<sup>a</sup> Caijin Xie,<sup>a</sup> Lili Yang<sup>a</sup> and Huiming Zhang<sup>a</sup>**

<sup>a</sup>*School of Physics and Astronomy, Sun Yat-Sen University, No.2 Daxue Rd, 519082, Zhuhai China*

*E-mail:* [shaochy@mail2.sysu.edu.cn](mailto:shaochy@mail2.sysu.edu.cn)

Neutrino Observatory in the Nanhai (NEON) is a proposed cubic-kilometer scale high-energy neutrino detector located in the South China Sea. One of its primary physical goals is to capture high-energy neutrinos, which could hint at the origin of cosmic rays. The detector performance is characterized by two parameters, effective volume and angular resolution. In this work, we first give a brief introduction to the design and structure of a digital optical module (DOM) that contains multiple PMTs. Based on the optimized configuration of the array, a maximum-likelihood reconstruction algorithm for sub-PeV simulated track-like events is developed and presented, which fully takes advantage of our array. The angular resolution and effective volume for muons are estimated, and the detector sensitivity to neutrino fluxes is evaluated. We show that NEON in the energy between 1 TeV to 1000 TeV can be competitive and advanced to current neutrino experiments.

38th International Cosmic Ray Conference (ICRC2023)  
26 July - 3 August, 2023  
Nagoya, Japan



---

\*Speaker

## 1. Introduction

The Neutrino Observatory in the Nanhai (NEON) is a deep-sea cubic-kilometer scale high-energy neutrino detector deployed in the South China Sea. It will be constructed at a depth of about 3-4 km. The experiment aims at detecting high-energy astrophysical neutrinos using a 3D array of 17-inch optical modules (OMs) housing 31 3-inch photo-multiplier tubes (PMTs). These OMs are arranged along vertical strings anchored on the seabed and pulled up by a buoy. Serving as the foundational components, the OMs capture and record the Cherenkov photons emitted by the secondary particles resulting from neutrino interactions.

Neutrino detection relies on two primary channels. The first channel involves cascade events triggered by charged current (CC) interactions of electron neutrinos ( $\nu_e$ ) and tau neutrinos ( $\nu_\tau$ ), as well as neutral current (NC) interactions across all neutrino flavors. The second channel is associated with track-like events that arise from charged current interactions of muon neutrinos ( $\nu_\mu$ ). These track-like events possess a distinct morphology, granting them excellent angular resolution, which is essential in the quest to identify neutrino origins from the diffuse neutrinos [1, 2].

In this study, we focus on the reconstruction algorithm for track-like events from Monte Carlo simulations with our array. In order to simulate the interaction of neutrinos with the surrounding medium, the gSeaGen package [3] developed by KM3NeT collaboration is utilized. The productions of this interaction are then injected into a 1 km<sup>3</sup> array that follows the Fibonacci sequence. We adopt the Geant4 [4] to construct the array and simulate the response of the detectors. The neutrino signals with energies ranging from 1 to 1000 TeV are simulated.

With the simulation result described above, we arrange the manuscript as follows. We describe our reconstruction algorithm of track-like events in details in Section 2. The reconstruction result and corresponding effective volume are then given in Section 3. The final conclusion is given in Section 4.

## 2. Muon Reconstruction

For muon tracks, there is an assumption that photons are only from Cherenkov radiation. Under this assumption, if we know the reaction position (vertex)  $\vec{P}(x, y, z)$  and propagation direction  $\vec{d}(\theta, \phi)$  of a muon neutrino in a detector, for hit  $i$ , we can calculate the residual time between the time  $t_{\text{the}}^i$  of each Cherenkov photon arriving at the detector and the true time  $t_{\text{det}}^i$  recorded by the detector,

$$t_{\text{res}}^i = t_{\text{det}}^i - t_{\text{the}}^i. \quad (1)$$

The residual time is important for muon reconstruction, and if it follows a distribution of  $\delta$  function, we will get a perfect fitting result.

However, there are several factors smearing its distribution. In the deep sea, most detected signals are attributed to noise rather than Cherenkov radiation. There are several sources of noise, including K40 decay [5], light emitted by organic matter, deep-sea fish as a biological response [6, 7], and PMT dark current. Furthermore, the scattering and absorption effects also cause a delay of  $t_{\text{det}}$ .

Among them, the K40 decay is the major contribution, and its decay process directly or indirectly produces relativistic electrons of  $\sim$  MeV, which then emit Cherenkov light to generate

optical background noise. To further explore it, we construct a water body with uniformly distributed K40 with a size of over one hundred meters for simulation. Finally, we obtained a counting rate of about 2.46 kHz for every 3-inch PMT.

The charge deposition of a single PMT resulting from a muon track is comparable to the noise level, typically around 1 photoelectron (1pe). Therefore, the first step is to distinguish and eliminate noise hits while preserving the signal hits. To achieve this, we apply an approach for selecting signal hits from the background, which successfully screens out more than 99 percent of K40 noise hits as described in Section 2.1.

For the selected hits, we utilize a likelihood fit combined with a full-sky scan method to determine the optimal set of parameters that best fit the observed data. Additionally, we employ a probability distribution function (PDF) to achieve a more precise angular reconstruction associated with the neutrino event. This helps to improve the accuracy of angular reconstruction and further refine our analysis.

## 2.1 Noise Exclusion

The presence of K40 noise in seawater introduces complexities in the reconstruction of signal hits. However, employing a filtering process enables us to effectively eliminate a significant portion of K40, simplifying the subsequent reconstruction process.

The direction and time of the signal hits are strongly correlated with each other, while the random K40 backgrounds show weak correlations. Considering this, we follow Trovato's work [8] to divide hits into different levels of score by evaluating their correlation. The hit with the highest score would be used as the starting point to construct the selection set. In the construction, hits that meet the following two conditions with the starting point will enter the selection sample.

$$|\Delta t| - \frac{\Delta r}{v} < 20\text{ns}, \quad \left| |\Delta t| - \frac{\Delta r}{c} \right| < 500\text{ns} \quad (2)$$

where  $\Delta t = t_{\text{hit}}^i - t_{\text{ref}}$ ,  $\Delta r = |\vec{p}_{\text{hit}}^i - \vec{p}_{\text{ref}}|$ . Only the selection sample with a size larger than 5 will be reconstructed. Under this selection, 99.9% of the starting point for the reconstructed event is the signal. As shown in Figure 1, this filtering process can help us screen out larger than 99 percent of K40.

A further filtering process could then be performed based on the direction information. For the OM with 31 PMTs, it is possible to infer the approximate direction of each hit. As muons tend to illuminate the PMTs directly facing them, while K40 noise exhibits isotropic illumination, a selection based on a rough estimation of the muon direction can be achieved. This selection process, illustrated in Figure 2, retains only the hits where  $\vec{d}_{\text{light}} \cdot \vec{d}_{\text{pmt}} > 0.5$ . The filter effectively eliminates photons that scatter in the water and occasionally hit the OM in the opposite direction. Considering that photons further from the muon tracks are more prone to scattering, an additional selection is performed. This selection includes hits with times ranging from -250 to 250 ns and a distance from the track of less than 100 m.

## 2.2 Track Reconstruction

The primary goal of event reconstruction is to ascertain the direction of the trajectory. The muon's trajectory can be characterized by five independent parameters, including the direction and

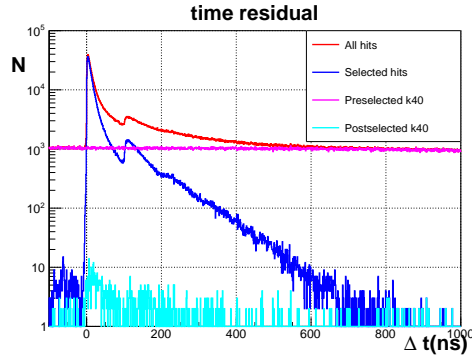


**Figure 1:** The time residual of signal and noise distribution. Reddish lines refer to the pre-selection, red line is all hits(signal+noise), and pink line is K40 noise. Blueish lines refer to the post-selection. Dark blue is selected hits and Cambridge blue line is K40 noise.

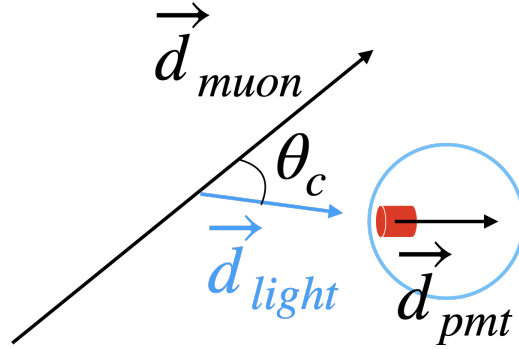


**Figure 2:** Sketch map of angular selection.

vertex coordinates. To achieve a more precise outcome, we perform the reconstruction process in three sequential steps.

### 2.2.1 Linear Fit

The first step in the track reconstruction procedure is the “linear fit”. For a muon event, its direction can be roughly determined by connecting the positions of hits along the trajectory. Although not very accurate, it has the advantage of no require of the starting point. After obtaining the screened hits, we use these hits to connect with each other according to the following formula,

$$\vec{d} = \sum_{ij(t_j > t_i)} w_{ij} \cdot (\vec{P}_j - \vec{P}_i), \quad w_{ij} = q_j + q_i \quad (3)$$

where  $q_i$  is photon electron detected by PMT for hit  $i$ . The linear fit follows a straightforward logic and provides a relatively rough estimation, yet it exhibits minimal deviation and possesses robust noise resilience. Its output direction serves as a suitable starting point for the subsequent accurate fitting process.

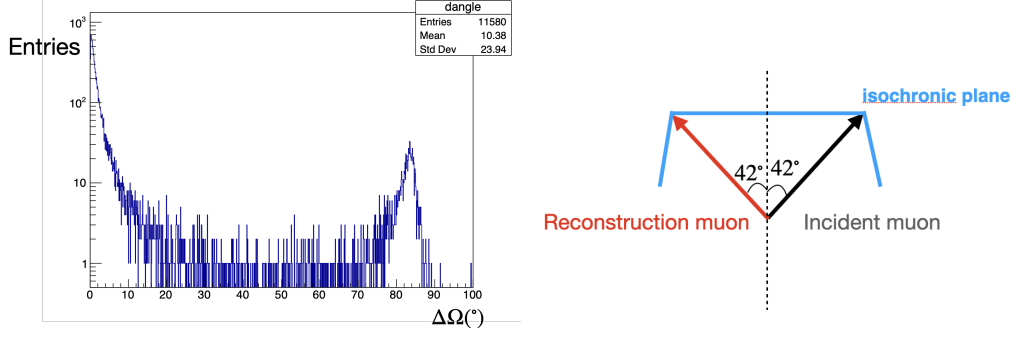


**Figure 3:**  $\Delta\Omega$  distribution. The x-axis is the included angle between the simulated and reconstruction muon direction. Sketch map of  $\Delta\Omega = 84^\circ$  event. When the direction of reconstruction muon and incident muon, part of their isochronic plane is coincident.

## 2.2.2 Chi-square Fitting

As introduced above, the residual time of each hit  $t_{\text{res}}^i$  can be calculated according to a defined track. A naive chi-square could be written as

$$\chi^2 = \sum_i (t_{\text{res}}^i)^2. \quad (4)$$

We can obtain  $\vec{P}(x, y, z)$  and  $\vec{d}(\theta, \phi)$  by optimizing this  $\chi^2$ . To achieve a globally optimized result, we perform 12288 local optimizations by initially aligning the directions according to the partitioning of HEALPix.

However, we encountered an issue with this method, as depicted in Figure 3, where the optimal fitting results fall into two regions. Notably, two peaks are observed around  $0^\circ$  and  $84^\circ$ , as illustrated in Figure 3. It is caused by symmetry about isochronous planes and the error. For a detailed explanation, please refer to Figure 3. To solve this problem, we employ the direction obtained from a linear fit as an initial starting point for the chi-square fitting process. Additionally, we introduce a 10-degree step and impose an upper limit on the number of iterations.

## 2.2.3 Probability Density Function

The next fitting procedure is based on the method of “maximum likelihood”. Considering the time residual  $t_{\text{res}}$  distributed with a probability density function (PDF) obtained from the Monte-Carlo samples, the likelihood function of parameters when observing a set of measurements is

$$L(t_{\text{res}}^1, t_{\text{res}}^2, \dots, t_{\text{res}}^n | \vec{P}, \vec{d}) = \prod_i f(t_{\text{res}}^i | \vec{P}, \vec{d}). \quad (5)$$

The values of the parameters can be determined by minimizing  $-\log L$ , and the parameter

$$\Lambda \equiv -\frac{\log L}{N_{\text{hit}} - 5} \quad (6)$$

is used as an indicator of the quality of reconstruction.

Although using the correct probability density function (PDF) in a likelihood fit has its advantages, it can be challenging to find the global maximum of the likelihood. This is because the PDF

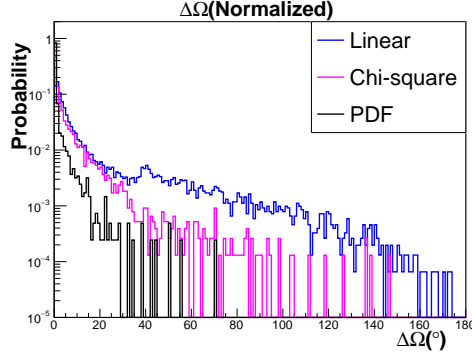


**Figure 4:** The directional reconstruction of three methods. Blue line is linear fit, pink line is chi square fit and black line is PDF fit. The result of each step is getting better.

becomes a relatively flat function for large time residual, which can lead to the appearance of local maxima in the likelihood function. Therefore, we use the result from the last step as a starting point to do this procedure. We compare the performance of these three steps in Figure 4.

### 3. Analysis and Results

In the previous chapter, we develop the fitting method. However, subsequent to that, selection criteria can be implemented based on the requirements of the specific physics analysis. In this section, we introduce a variable that can be employed to discard poorly reconstructed events.

A straightforward approach to distinguish between good and poor events is to cut on the value of the parameter  $\Lambda$  defined in Equation 6. The event with a  $\Delta\Omega < 1^\circ$  and  $\Delta\Omega > 1^\circ$  have a different distribution with  $\Lambda$ . To evaluate the performance of the selection, we adopt the parameters True Positive Rate (TPR) and False Positive Rate (FPR),

$$\text{TPR} \equiv \frac{N_{\Delta\Omega < 1^\circ}^{\text{cut}}}{N_{\Delta\Omega < 1^\circ}}, \text{FPR} \equiv \frac{N_{\Delta\Omega > 1^\circ}^{\text{cut}}}{N_{\Delta\Omega > 1^\circ}}. \quad (7)$$

By analyzing the TPR and FPR values for different cut conditions, we determined that the optimal cut condition is  $\Lambda < 3.9$ , where the TPR – FPR difference is maximized. With this cut condition, we are able to retain approximately 76% of good events while successfully rejecting around 64% of bad events.

After selecting the events, we proceed to calculate the angular resolution for various energy bins, as shown in Fig. 5. The angular resolution is around  $0.15^\circ$  when the energy is up to 100 TeV.

The effective volume of a detector is another important performance indicator for measuring the event rate. The effective volume of high-energy neutrinos with different energies can be obtained by simulation, and the corresponding formula is

$$V_{\text{eff}} = V_{\text{sample}} * \frac{N_{\text{rec}}}{N_{\text{sample}}} \quad (8)$$

where  $N_{\text{sample}}$  is the number of primary event points in the simulation,  $V_{\text{sample}}$  is the volume of the primary event point, and  $N_{\text{rec}}$  is the number of reconstruction events. The Effective volume of NEON is shown in Fig. 5.

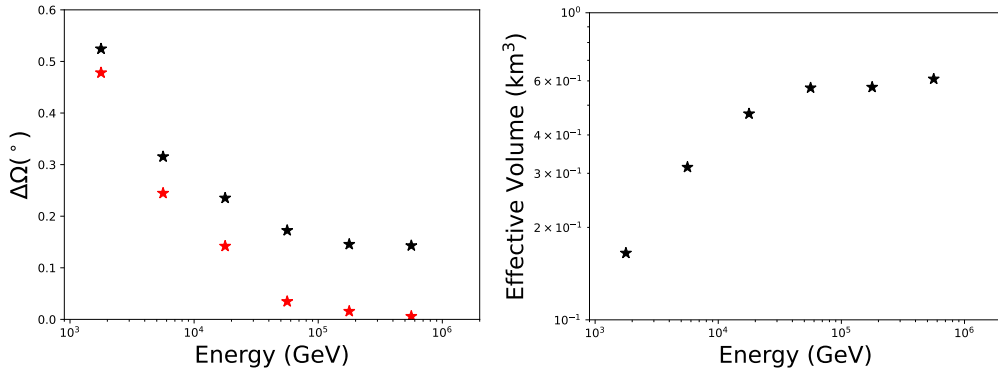


**Figure 5:** Left panel: Median angular error as function of the neutrino true energy. The black dots refer to the angle between the reconstructed track and neutrino true direction, and the red dots refer to the median angle between the true neutrino and muon directions. Right panel: Effective volume as function of the neutrino true energy.

#### 4. Conclusion

In this study, based on the configuration of NEON we study the detection performance. We examine the impact of K40 noise and evaluate the effectiveness of the hits selection method. We performed angular reconstruction analysis on muon neutrino ( $\nu_\mu$ ) track-like events. Based on the photon arrival time measured by OMs, we used the maximum likelihood estimation method to reconstruct the direction of the track. The algorithm comprises three sequential steps: Linear fit, Chi-square Fit, and PDF fit. The output of each step serves as the starting point for the subsequent step, resulting in cumulative improvements. Our reconstruction results show that the angular resolution of NEON above 1 TeV  $\nu_\mu$  can reach within 0.7 degrees, while for 100 TeV  $\nu_\mu$ , it can reach about 0.15 degrees. We analyzed the effective volume of  $\nu_\mu$  in NEON, and through sampling and filtering of complete events, we obtained an effective volume of about 0.6 km<sup>3</sup> at 100 TeV.

#### 5. Acknowledgements

This work is supported by the National Natural Science Foundation of China (NSFC) grants 12005313, 12205388, 12261141691 and 42150105.

## References

- [1] Ke Fang, Kumiko Kotera, M. Coleman Miller, Kohta Murase, and Foteini Oikonomou. Identifying Ultrahigh-Energy Cosmic-Ray Accelerators with Future Ultrahigh-Energy Neutrino Detectors. *Journal of Cosmology and Astroparticle Physics*, 2016(12):017–017, December 2016. ISSN 1475-7516. doi: 10.1088/1475-7516/2016/12/017. URL <http://arxiv.org/abs/1609.08027>. arXiv:1609.08027 [astro-ph, physics:hep-ph].
- [2] IceCube Collaboration\*†, R Abbasi, M Ackermann, J Adams, JA Aguilar, M Ahlers, M Ahrens, JM Alameddine, AA Alves Jr, NM Amin, et al. Observation of high-energy neutrinos from the galactic plane. *Science*, 380(6652):1338–1343, 2023.
- [3] Sebastiano Aiello, Arnauld Albert, S Alves Garre, Zineb Aly, Fabrizio Ameli, Michel Andre, Giorgos Androulakis, Marco Anghinolfi, Mancia Anguita, Gisela Anton, et al. gseagen: The km3net genie-based code for neutrino telescopes. *Computer Physics Communications*, 256: 107477, 2020.
- [4] Sea Agostinelli, John Allison, K al Amako, John Apostolakis, H Araujo, Pedro Arce, Makoto Asai, D Axen, Swagato Banerjee, GJNI Barrand, et al. Geant4—a simulation toolkit. *Nuclear instruments and methods in physics research section A: Accelerators, Spectrometers, Detectors and Associated Equipment*, 506(3):250–303, 2003.
- [5] Bjoern Herold, KM3NeT Consortium, et al. Study of 40k-induced rates for a km3net design option with multi-pmt optical modules. *Nuclear Instruments and Methods in Physics Research Section A: Accelerators, Spectrometers, Detectors and Associated Equipment*, 626:S234–S236, 2011.
- [6] N Reeb, S Hutschenreuter, P Zehetner, T Ensslin, S Alves, M André, M Anghinolfi, G Anton, M Ardid, J-J Aubert, et al. Studying bioluminescence flashes with the antares deep sea neutrino telescope. *arXiv preprint arXiv:2107.08063*, 2021.
- [7] VA Allakhverdyan, AD Avrorin, AV Avrorin, VM Aynutdinov, R Bannasch, Z Bardáčová, IA Belolaptikov, IV Borina, VB Brudanin, NM Budnev, et al. The baikal-gvd neutrino telescope as an instrument for studying baikal water luminescence. *arXiv preprint arXiv:2107.14211*, 2021.
- [8] Agata Trovato. Development of reconstruction algorithms for large volume neutrino telescopes and their application to the km3net detector. 2014.